Influence of Paving Interlayer Material on Performance of Full-Scale Asphalt Overlays

V. Vinay Kumar, Ph.D., M.ASCE[1]; Gholam H. Roodi, Ph.D.[2];
and Jorge G. Zornberg, Ph.D., P.E., F.ASCE[3]

[1]Technical Manager, Pavements, Huesker Inc., Austin, TX. Email: vkumar@huesker.com
[2]Geotechnical Designer, HDR, Toronto, ON. Email: gholamhossein.roodi@hdrinc.com
[3]Professor, Dept. of Civil, Architectural, and Environmental Engineering, Univ. of Texas at Austin, Austin, TX. Email: zornberg@mail.utexas.edu

ABSTRACT

The influence of two paving interlayer materials on the performance of asphalt overlays is evaluated in this study. Specifically, a series of controlled traffic loadings were conducted on an unreinforced (no paving interlayer) and two reinforced, sensor-instrumented asphalt overlay sections constructed during the rehabilitation of the Texas State Highway (SH) 21. The two paving interlayer materials used in the reinforced asphalt overlay sections included polyester composite reinforcement (PET) and fiberglass composite reinforcement (FG) products. The rehabilitation of SH21 involved repairing the pre-existing asphalt, placing a binder tack coat, installing a paving interlayer (except in the unreinforced section), and finally constructing a 75-mm thick asphalt overlay. Controlled traffic loadings were conducted, which involved driving standard axle loads directly above asphalt strain gauges that had been installed at mid-depth of the pre-existing asphalt layer. Comparison of tensile strains recorded under standard axle loads among the unreinforced and two reinforced asphalt overlay sections revealed significantly smaller tensile strains in the reinforced asphalt overlay sections. Between the two reinforced asphalt overlay sections, the tensile strains were consistently lower for the overlay section with PET product compared to that with FG product. Overall, the paving interlayers evaluated in this study significantly reduced the tensile strains under standard axle loads indicating a potential increase in the roadway structural capacity.

Keywords: *Asphalt overlay, Polyester composite, Fiberglass composite, Sensor-instrumentation, Roadway structural capacity.*

INTRODUCTION

Geosynthetics of different forms and materials have been used as paving interlayers for main objectives of retarding (or minimizing) reflective cracks and water proofing (e.g., Lytton 1989; Zornberg 2017; Solatiyan et al. 2020; Kumar et al. 2021b). More recent research studies have indicated that geosynthetic interlayers can also provide increased structural capacity to pavement (e.g., Correia and Zornberg 2016, 2018; Kumar et al. 2021b, 2022). However, quantification of such increases in the pavement structural capacity has been very limited. A relevant measurement for evaluation of structural capacity of pavements is the tensile strain at the bottom of the hot mix asphalt (HMA) layer induced by the traffic load.

Benefits from geosynthetic interlayers have been studied by adopting a wide range of experimental setups (e.g., Virgili et al. 2009; Correia and Zornberg 2016; Kumar and Saride 2017; Saride and Kumar 2019; Roodi et al. 2017; Spadoni et al. 2021; Canestrari et al. 2022;

Kumar et al. 2021b) as well as numerical studies and field investigations (e.g., Kwon et al. 2005; Laurinavicius and Oginskas 2006; Abdesssemed et al. 2015; Imjai et al., 2019; Kazimierowicz-Frankowska 2020; Kumar et al., 2021a). The emphasis of most research programs has been on quantifying the ability of geosynthetic interlayers to restrict reflecting pre-existing cracks from an old asphalt layer into a newly built overlay. Despite consensus on the benefits from geosynthetic interlayers, conditions and specifications that determine the suitability of various geosynthetics used as interlayers has still remained unclear. Specifically, the difference between the performance of polymeric versus fiberglass materials, which constitute the two main synthetic materials for geosynthetic interlayers, has not clearly been understood.

This paper presents the results obtained in a field investigation that was focused on evaluating benefits from geosynthetic interlayer in increasing the pavement structural capacity. For this purpose, the tensile strains at the bottom of the HMA layer induced by a standard axle load was measured in several field test sections that were constructed with various designs. Among the various designs, to evaluate performance of polymeric against fiberglass interlayers, this paper focuses only on the data obtained in two reinforced test sections that had polymeric and fiberglass interlayers from the same manufacturer. The tensile strain in the two reinforced sections is compared to the tensile strain obtained in an unreinforced test section with the same design. A brief project background is presented next and then the tensile strain data obtained in the three test sections are presented and discussed.

PROJECT BACKGROUND

As part of a rehabilitation program along the Texas State Highway (SH) 21, Texas Department of Transportation (TxDOT) performed half- or full-depth road repairs followed by the installation of a 20 mm thick level-up asphalt course. In addition, a geosynthetic-reinforced asphalt overlay was built, which was made by applying tack coat on the level-up asphalt, installing a geosynthetic interlayer atop the tack coat, and finally, constructing an asphalt overlay that comprised of two lifts: a 50 -mm- thick dense-graded asphalt mix referred to as TY-D, overlain by a 25- mm- thick thin-overlay mixture referred to as TOM, as shown in Fig. 1 (Kumar et al. 2023).

In coordination with the University of Texas at Austin, TxDOT allocated a portion of the road to a field experimental program where a wide range of geosynthetic interlayers with various forms and materials were tested. Specifically, four different polymeric interlayers and five different fiberglass interlayers were installed along a 1.34-km-long stretch of the road in 32 experimental test sections (Kumar et al. 2023). Among others, seven test sections (including six geosynthetic-reinforced sections and one unreinforced section) were instrumented in the subgrade, base, subbase, and the HMA layers, using a comprehensive set of sensors including moisture sensors, geophones, asphalt strain gauges (ASGs), and thermocouples. Within each of the seven test sections, three ASGs were installed along the wheel path including two ASGs (duplicates) to measure tensile strains in the direction transverse to traffic (referred to here as the transverse ASGs) and one ASG to measure tensile strains along the traffic direction (referred to here as the longitudinal ASG). All ASGs were installed at locations where the pre-existing asphalt was intact to allow quantification of the impact of the geosynthetic reinforcements on the roadway structural capacity, rather than mitigating reflective cracking.

This paper presents the tensile strain recorded by the transverse ASGs in three test sections including an unreinforced test section and two test sections that were reinforced using polymetric

and fiberglass reinforcements from a single manufacturer. The reported tensile strain data corresponds to one of the two duplicate transverse ASGs in each test section, while the data from the other transverse ASG was used for validation.

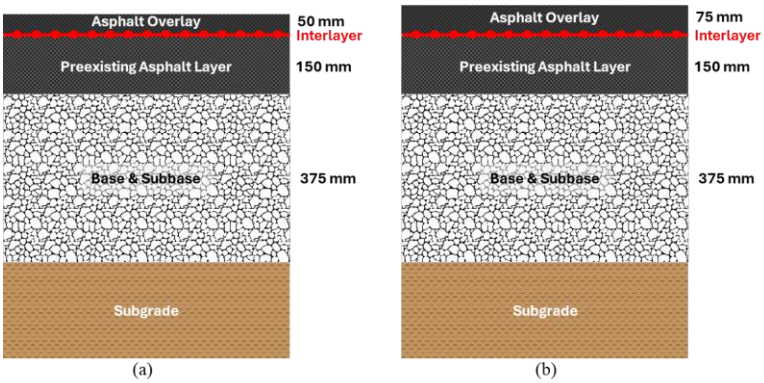

Figure 1. Roadway cross-sections with: (a) 50-mm-thick overlay; (b) 75-mm-thick overlay.

MATERIALS

Tack Coat & Asphalt Mixture. Two different types of tack coats including a polymer modified asphalt cement (AC-15P) and a cationic, slow-setting, low-viscosity, comparatively hard residue emulsion (CSS-1H) were used in this study. Specifically, AC-15P at an application rate of 0.54 l/m^2 was applied as a tack coat on the pre-existing asphalt in sections with paving interlayers. While CSS-1H at an application rate of 0.27 l/m^2 was applied as a tack coat on the pre-existing asphalt in sections without paving interlayers (control section). Additionally, CSS-1H at an application rate of 0.27 l/m^2 was applied as a tack coat between TY-D and TOM layers in all the sections. The asphalt overlay in this study comprised of two lifts of asphalt mixture that included a dense-graded asphalt mixture, referred to as TY-D, and a thin wearing-course asphalt mixture referred to as TOM. The maximum aggregate sizes in the TY-D and TOM mixtures were 20 mm and 12.5 mm, respectively. The TY-D mixture comprised a Performance Grade (PG) 64-22 binder at an optimum binder content of 5.2%, while the TOM comprised a PG 76-22 binder at an optimum binder content of 6%. Additionally, a warm mix additive (Evotherm) was added at a rate of 0.4% by weight of aggregates for use as a compaction aid in both asphalt mixtures.

Paving Interlayers. Multiple paving interlayers that provided reinforcement function were used as asphalt reinforcements in this research study. However, within this research paper, two of the many paving interlayers were considered, which included a polyester (PET) geogrid composite and a fiberglass (FG) geogrid composite. While the variety of geosynthetic interlayers is significant, this study did not focus on other interlayer functions or mechanisms such as barrier or stress relief. Additionally, both the paving interlayer products discussed herein were selected from the same manufacturer, considering their material composition, tensile and physical characteristics. The polyester geogrid composite referred herein as PET is a geogrid manufactured with high modulus polyester yarns combined with an ultra-lightweight non-woven fabric and coated with a binder. The PET product has a mass per unit area of 270 g/m^2, an aperture size of 40 mm × 40 mm, and an ultimate tensile strength of 50 kN/m at an elongation of about 10%. The fiberglass geogrid composite referred herein as FG is a geogrid made of glass

fibers combined with an ultra-thin non-woven fabric and coated with a binder. The FG product has a mass per unit area of 596 g/m^2, an aperture size of 30 mm × 30 mm, and an ultimate tensile strength of 100 kN/m at an elongation of about 3%. The asphalt retention capacity of both the products were about 0.47 l/m^2. Additional details including the rest of paving interlayers evaluated in the research project are provided in Kumar et al. (2022, 2023).

CONTROLLED TRAFFIC LOADING

The influence of paving interlayers along with the asphalt overlay type and thickness on the performance of full-scale asphalt overlay sections were evaluated using field data collected from ASGs as part of controlled traffic loading campaigns performed in the three test sections considered in this study. Specifically, controlled traffic loadings were performed on three sensor-instrumented test sections after construction of the 50-mm-thick TY-D layer, referred to as 50-mm-thick overlay (see Fig. 1(a)). In addition, controlled traffic loadings were conducted after construction of the additional 25-mm-thick TOM layer, referred to as 75-mm-thick overlay (see Fig. 1(b)). Each controlled traffic loading included a minimum of 10 passes at an average speed of 40 kph. In each pass, the tensile strain reading was set to zero and the maximum tensile strain induced by the traffic was determined. The maximum tensile strains were compared among multiple passes before representative values for each test section were selected. Additional controls including video recording was also adopted to accurately capture the wheel path in each pass. Detailed information on the instrumentations and loading campaigns are presented by Kumar et al. (2022, 2023). The tensile strain results recorded from three test sections considered in this study are discussed in the following sections.

RESULTS & DISCUSSION

Peak Tensile Strains. A typical tensile strain response obtained from the ASGs in the control section under a standard axle load applied on the 50-mm-thick overlay is presented in Fig. 2. As shown in the figure, three distinct peaks representing three axles of the loaded-dump truck (i.e., standard axle load) were obtained. It can also be observed that the tensile strains under the front axle load is comparatively higher than that under the rear axle loads, owing to the change in widths of front and rear axles. Additionally, among the two rear axles, the tensile strains under the second rear axle were higher than the first rear axle. This may be due to the variations in the loads and tire pressures between the two rear axles. Subsequently, the peak tensile strains recorded for different axle loads (i.e., front, and rear axles) from different traffic loadings applied on 50 and 75-mm-thick overlays in three test sections considered in this study are plotted as a ‘Box and Whisker’ plot as shown in Figs. 3a and b, respectively.

Box and Whisker plots represent the variations in peak tensile strains for multiple passes of standard axle loads including front and rear axles applied on both 50 and 75-mm-thick overlay configurations in three test sections. Specifically, the top and bottom whiskers represent the maximum and minimum values respectively, while the upper and lower portions of the box represent the upper and lower quartiles respectively. Additionally, the line dividing the box represents the median value, and the cross-mark represents the mean value of the peak tensile strains recorded from traffic loadings. As shown in the figure (see Fig. 3(a)), the range of peak tensile strains in control section were consistently higher than that in the reinforced sections, irrespective of the axle loads (i.e., front, rear). For instance, the peak tensile strains in control

section with 50-mm-thick overlay configuration under front axle loads ranged from 480 μm/m to 590 μm/m, while the range for reinforced sections were about 90 μm/m to 230 μm/m (PET) and 160 μm/m to 290 μm/m (FG). While the ranges of peak tensile strains under the first rear axle loads were about 160 μm/m to 330 μm/m (CS), 30 μm/m to 110 μm/m (PET), and 50 μm/m to 160 μm/m (FG), respectively. Slightly higher amplitudes with similar trends could be observed under second rear axle loads as well. The variations in tensile strain amplitudes under different axle loads maybe due to the tire configurations in each axle of the loaded dump-truck. Additionally, similar trends as 50-mm-thick overlay configuration, but with lower amplitudes could be observed for control and reinforced sections with 75-mm-thick overlay configuration (see Fig. 3(b)). Such lower amplitudes of peak tensile strain are due to the increased overlay thickness of 25 mm (i.e., from 50 mm to 75 mm). Subsequently, to compare the peak tensile strains between control and reinforced sections for different overlay configurations, mean values of peak tensile strains were determined, which is discussed next.

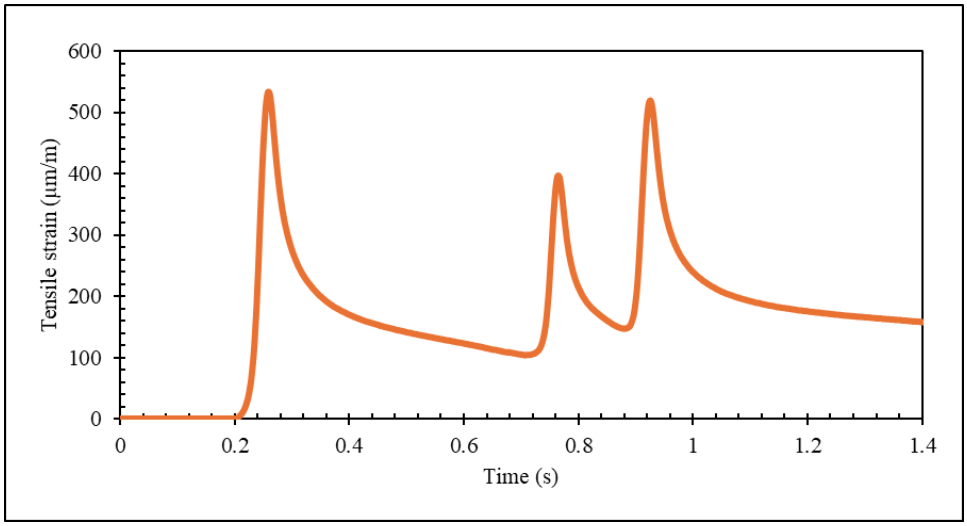

Figure 2. Tensile strain response under standard axle load.

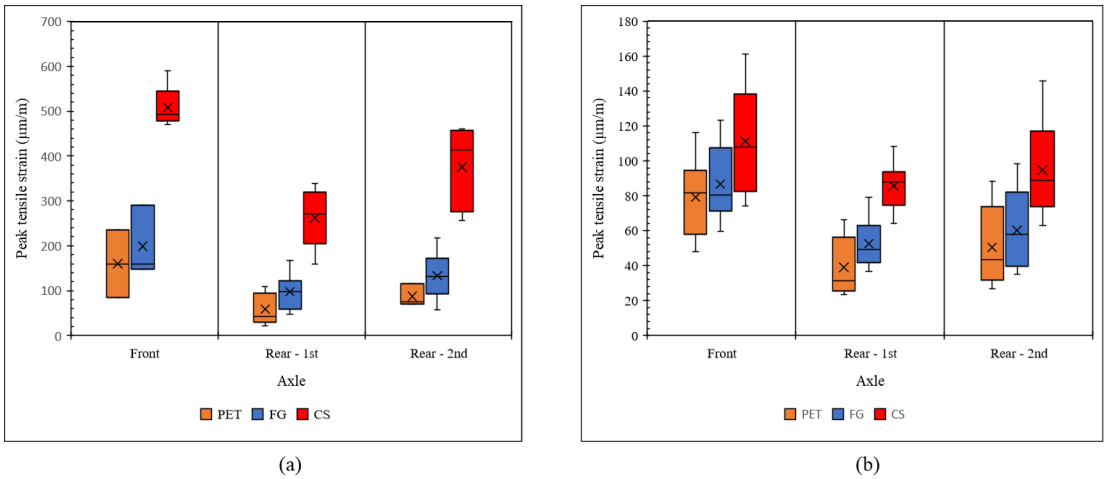

Figure 3. Box and whisker plots presenting peak tensile strains under standard axle loads applied on: (a) 50-mm-thick overlay; (b) 75-mm-thick overlay.

Mean of Peak Tensile Strains. Fig. 4 presents the mean of peak tensile strains in control and reinforced sections with 50 and 75-mm-thick overlays under front and rear axle loads. As shown in the figure, it is apparent that the tensile strains in the control section are consistently higher than those in the reinforced sections, irrespective of the overlay thickness (50 and 75-mm-thick) or the applied axle loads (Front or Rear). For instance, the results in Fig. 4(a) indicate that a tensile strain of 510 μm/m was reached in the control section, but significantly lower peak tensile strains were obtained in the geosynthetic-reinforced sections under the front axle loads applied on 50-mm-thick overlay (160 μm/m in PET and 200 μm/m in FG). This corresponds to reductions in tensile strain of approximately 69%, and 61% in test sections reinforced with PET and FG respectively. Figs. 4(b) & 4(c) present similar trends for the first and second rear axle loads applied on 50 and 75-mm-thick overlays, but with slightly lower amplitudes. For instance, tensile strains under first rear axle loads applied on the 50-mm-thick overlay were recorded to be on the order of 262 μm/m (CS), 59 μm/m (PET), and 97 μm/m (FG) respectively. While those under second rear axle loads were recorded to be on the order of 375 μm/m (CS), 87 μm/m (PET), and 132 μm/m (FG) respectively, with slightly higher amplitudes than those under first rear axle loads. These results display that the tensile strains recorded under the front axle loads were higher than those recorded under the second rear axle loads than those recorded under the first rear axle loads, irrespective of the overlay thickness.

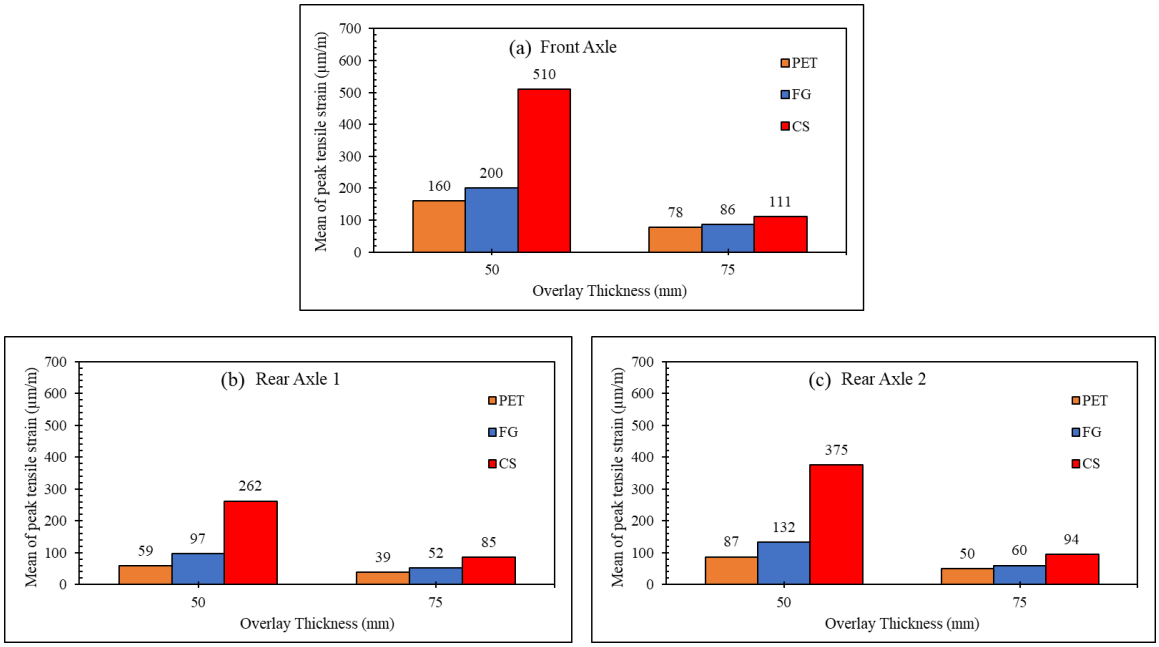

Figure 4. Variation of mean of peak tensile strains with overlay thickness under: (a) Front axle load; (b) First rear axle load; (c) Second rear axle load.

On the other hand, the results shown in Figs. 4(a), 4(b) & 4(c) also show the tensile strains in all the test sections considered in this study decrease with increasing asphalt thickness, irrespective of presence or not of paving interlayers. For instance, as revealed by the results in Fig. 4a, the tensile strains in the control section with 50-mm-thick overlay (510 μm/m) are significantly higher than those in the control section with 75-mm-thick overlay (111 μm/m), which corresponds to an approximate reduction of 78% in strains due to the additional overlay

thickness of 25 mm (TOM layer). Similar trends can be observed in the case of reinforced sections with about 55% reduction in strains due to the additional overlay thickness of 25 mm (TOM layer). However, the benefits (tensile strain reduction) due to paving interlayer was approximately 60% smaller for 75-mm-thick overlay in relation to 50-mm-thick overlay. Similar trends can be observed for the rear axle loads applied on 75-mm-thick overlay as shown in Figs. 4(b) & 4(c). These results also demonstrate that the inclusion of paving interlayers considered in this study, when placed at the interface between the pre-existing and new asphalt layers are effective in reducing the tensile strains under traffic loads. However, such benefit depends on the actual thickness and quality of the asphalt overlay. Accordingly, a comparatively small benefit may be expected when using a comparatively thick, high quality asphalt layer, at least immediately after placement of the asphalt overlay.

Adopting a comparatively thin layer of reinforced asphalt would not only result in reduced construction costs, but it would also lead to a more efficient geosynthetic reinforcement. On the other hand, the incorporation of paving interlayers in projects involving a comparatively thick layer of reinforced asphalt will still capitalize on the geosynthetic benefits, but only after degradation of the thick asphalt layer. However, it should be highlighted that the two paving interlayers evaluated in this study were effective in minimizing the tensile strains under both front and rear axle loads of a loaded dump-truck (i.e., standard axle load), leading to an enhanced performance of the pavement system. Among the sections with paving interlayers, tensile strains in PET-reinforced section were consistently lower than that in the FG-reinforced section. To further quantify the improvement in terms of tensile strain reductions in the two reinforced sections against the control section, the tensile strain reduction ratio is introduced as a performance indicator, as discussed in the following section.

Tensile Strain Reduction Ratio (α). The tensile strain reduction ratio (α) maybe defined as the ratio between the mean of peak tensile strains in a reinforced section to that in the control section, irrespective of the axle loads and overlay thicknesses. Accordingly, a tensile strain reduction ratio of comparatively small magnitude represents a significant reduction in tensile strain (i.e., enhanced performance corresponds to low 'α' values). The tensile strain reduction ratios for the two reinforced sections considered in this study are presented in Figs. 5(a), 5(b) & 5(c) for the front axle, first, and second rear axle loads, respectively. The results shown in the figures indicate that the tensile strain reduction ratios for loads applied on 50-mm-thick overlay are consistently smaller than the ratios corresponding to loads applied on 75-mm-thick overlay, irrespective of the applied axle loads. For instance, the tensile strain reduction ratios under front axle load range from 0.31 to 0.39 for 50-mm-thick overlay, and from 0.70 to 0.77 for 75-mm-thick overlay (see Fig. 5(a)). While the tensile strain reduction ratios under first and second rear axle loads range from 0.23 to 0.35 and 0.23 to 0.35 for 50-mm-thick overlays, and 0.46 to 0.61 and 0.53 to 0.64 for 75-mm-thick overlays, respectively. Additionally, it is evident that the tensile strain reduction ratios were consistently lower for the rear axle loads compared to the front axle loads, irrespective of the overlay thickness. This may be due to the impact of dual-tires and tandem axle configurations of the rear axles. These results indicate that the tensile strain reduction ratios depend on the overlay thickness, axle loads, and tire-configurations. However, among the sections reinforced with paving interlayers, significantly lower tensile strain reduction ratios were determined for PET-reinforced section in comparison with the FG-reinforced section. Such significant performance of PET-reinforced section can be attributed primarily to the tensile strength, tensile stiffness, and interface bonding of the PET paving interlayer. Specifically, the comparatively lower tensile stiffness of PET product compared to that with the FG product

makes it ductile and more resilient to the pre-existing surface conditions (e.g., oxidized, milled), installation and construction damages, while the FG products are brittle and hence, less resilient to installation and construction damages.

The stiffness of asphalt overlay may have also slightly influenced the magnitude of the tensile strain reduction ratios of the two reinforced sections evaluated in this study. The benefits that result from using reinforcements appear to be maximized when the stiffness of asphalt layer is comparatively low. Overall, it can be inferred that all the reinforced sections considered in this study showed a clearly superior structural capacity to that of the control section, as evidenced by the reduced tensile strains under front and rear axle loads applied on 50 and 75-mm-thick overlays. The tensile strain reduction ratios determined from geosynthetic-reinforced sections considered in this study may be adopted as part of the pavement design to reduce the asphalt overlay thickness and/or extend the service life without compromising the overall performance of the pavement system. The performance of such a flexible pavement system with reduced thickness and an extended service life is expected to be ultimately verified under the framework of a Mechanistic-Empirical Pavement Design approach.

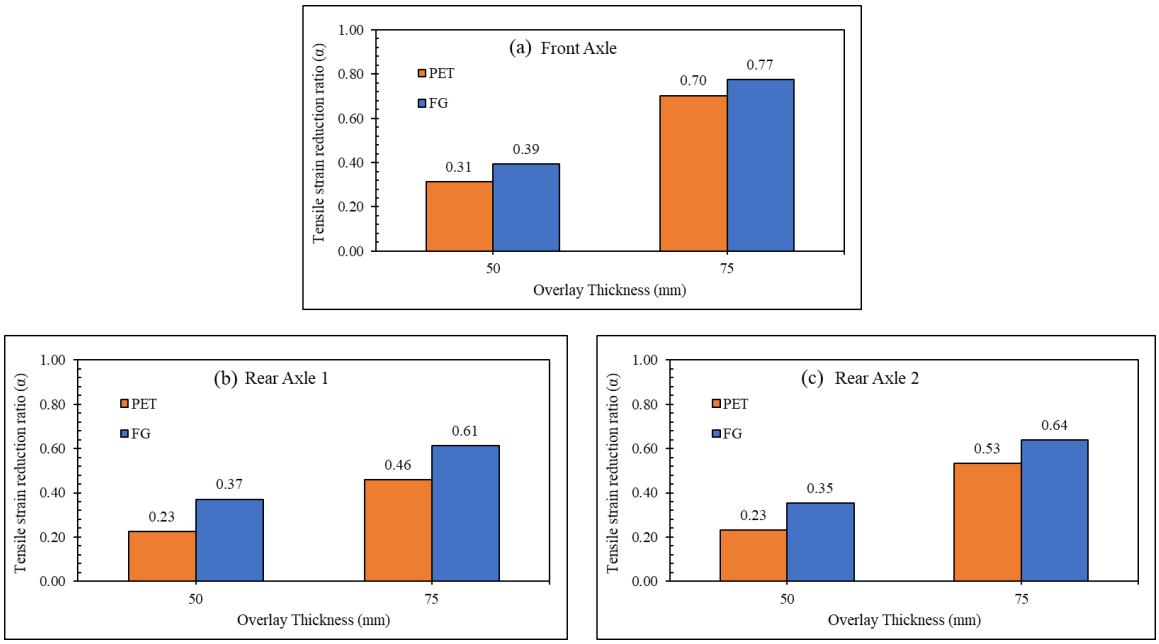

Figure 5. Variation of tensile strain reduction ratios with overlay thickness under: (a) Front axle load; (b) First rear axle load; (c) Second rear axle load.

CONCLUSIONS

The influence of paving interlayer materials on the performance of full-scale asphalt overlays built along the Texas State Highway (SH) 21 were evaluated by applying controlled traffic loadings via loaded dump-trucks in this study. Following conclusions could be drawn from the study:

The variations in peak tensile strains recorded from different traffic loadings could be efficiently presented via Box and Whisker plots, as shown in this study. The tensile strains in all the sections reinforced with paving interlayers were found to be significantly lower than that in

the control section. Specifically, the reductions in tensile strain of about 69% and 61% were determined respectively for PET and FG-reinforced sections with 50-mm-thick overlay. Among the reinforced sections, tensile strains in the PET-reinforced section were found to be consistently lower those recorded in the FG-reinforced section, irrespective of the asphalt overlay thickness and axle loads applied. Specifically, the tensile strains in PET-reinforced sections were about 20% to 40% lower than that in FG-reinforced sections with 50-mm-thick overly. The tensile strain reduction ratios ranged from 0.31 (PET) to 0.39 (FG) and from 0.70 (PET) to 0.77 (FG) for front axle loads applied on 50 and 75-mm-thick overlays, respectively. Additionally, for rear axle loads applied on 50 and 75-mm-thick overlays, these values ranged from 0.23 (PET) to 0.37 (FG) and 0.46 (PET) to 0.61 (FG) respectively. These trends indicate that the tensile strain reduction ratios are affected by overlay thickness, axle loads, and tire-configurations. Overall, the paving interlayers considered in this study were found to reduce the tensile strains effectively compared to the control section and enhance the roadway structural capacity. The tensile strain reduction ratios determined from geosynthetic-reinforced sections considered in this study may be adopted as part of the pavement design to reduce the asphalt overlay thickness and/or extend the service life without compromising the overall performance of the pavement system.

REFERENCES

Abdesssemed, M., Kenai, S., and Bali, A. 2015. Experimental and numerical analysis of the behavior of an airport pavement reinforced by geogrids. *Construct. Build. Mater.* 94, 547–554.

Canestrari, F., Cardone, F., Gaudenzi, E., Chiola, D., Gasbarro, N., and Ferrotti, G. 2022. Interlayer bonding characterization of interfaces reinforced with geocomposites in field applications. *Geotext. Geomembranes* 50 (1), 154–162.

Correia, N. S., and Zornberg, J. G. 2016. Mechanical response of flexible pavements enhanced with geogrid-reinforced asphalt overlays. *Geosynth. Int.* 23 (3), 183–193.

Correia, N. S., and Zornberg, J. G. 2018. Strain distribution along geogrid-reinforced asphalt overlays under traffic loading. *Geotext. Geomembranes* 46, 111–120.

Imjai, T., Pilakoutas, K., and Guadagnini, M. 2019. Performance of geosynthetic-reinforced flexible pavements in full-scale field trials. *Geotext. Geomembranes* 47, 217–229.

Kazimierowicz-Frankowska, K. 2020. Influence of geosynthetic reinforcement on maximum settlements of semi-rigid pavements. *Geosynth. Int.* 27 (4), 348–363.

Kumar, V. V., Roodi, G. H., and Zornberg, J. G. 2021a. Asphalt strain response of geosynthetic-reinforced asphalt overlays under static plate loads. *Geosynthetics Conference 2021*. Kansas City, Kansas, USA, pp. 350–361.

Kumar, V. V., Roodi, G. H., Subramanian, S., and Zornberg J. G. 2022. Influence of asphalt thickness on performance of geosynthetic-reinforced asphalt: Full-scale field study. *Geotext. Geomembranes* 50, 1052–1059.

Kumar, V. V., Roodi, G. H., Subramanian, S., and Zornberg J. G. 2023. Installation of geosynthetic interlayers during overlay construction: Case study of Texas State Highway 21. *Transport. Geotech.* 43, 101127.

Kumar, V. V., and Saride, S. 2017. Evaluation of Flexural Fatigue Behavior of Two-Layered Asphalt Beams with Geosynthetic Interlayers Using Digital Image Correlation. *Transportation Research Board 96th Annual Meeting*, Washington DC, USA, pp. 8–12.

Kumar, V. V., Saride, S., and Zornberg, J. G. 2021b. Mechanical response of full-scale geosynthetic-reinforced asphalt overlays subjected to repeated loads. *Transport. Geotech.* 30, 100617.

Kwon, J., Tutumluer, E., and Kim, M. 2005. Development of a mechanical model for geosynthetic-reinforced flexible pavements. *Geosynth. Int.* 12 (6), 310–320.

Laurinavicius, A., and Oginskas, R. 2006. Experimental research on the development of rutting in asphalt concrete pavements reinforced with geosynthetic materials. *J. Civ. Eng. Manag.* 12 (4), 311–317.

Lytton, R. L. 1989. Use of geotextiles for reinforcement and strain relief in asphalt concrete. *Geotext. Geomembranes* 8 (3), 217–237.

Roodi, G. H., Morsy, A. M., and Zornberg, J. G. 2017. Experimental evaluation of the interaction between geosynthetic reinforcements and hot mix asphalt. *International Conference on Airfield and Highway Pavements*. ASCE, Philadelphia, Pennsylvania, USA, pp. 428–439.

Saride, S., and Kumar, V. V. 2019. Estimation of service life of geosynthetic-reinforced asphalt overlays from beam and large-scale fatigue tests. *J. Test. Eval.* 47 (4), 2693–2716.

Solatiyan, E., Bueche, N., and Carter, A. 2020. A review on mechanical behavior and design considerations for reinforced-rehabilitated bituminous pavements. *Construct. Build. Mater.* 257, 119483.

Spadoni, S., Ingrassia, L. P., Paoloni, G., Virgili, A., and Canestrari, F. 2021. Influence of geocomposite properties on the crack propagation and interlayer bonding of asphalt pavements. *Materials* 14 (8), 5310.

Zornberg, J. G. 2017. Functions and applications of geosynthetics in roadways. *Procedia Eng.* 189, 298–306.